Starlight beneath the waves : in search of TeV photon emission from Gamma-Ray Bursts with the ANTARES Neutrino Telescope

Laksmana-Astraatmadja, T.

5 *Muon event rate and discovery potential from stacked GRB events*

From the results in Chapter 4, we could now investigate how long do we have to wait before a sufficiently nearby GRB event takes place, or in another words, how frequent can we observe a GRB with $z \lesssim 0.1$? Aside from this question, a second aim of this Chapter is to calculate the integrated muon flux of any number of simulated GRB events. To do this, a Monte Carlo method to simulate GRB events is developed, using a distribution functions of several GRB parameters. These distribution functions are known collectively as the GRB world model (Butler, Bloom & Poznanski, 2010).

5.1 GRB world model

The study of GRBs distribution functions has been intensified due to the wealth of data from *Swift*. The latest data release contains 425 bursts in which 147 of them have a measured redshift. This data set largely supersedes previous GRB analyses (Butler et al., 2007; Butler, Bloom & Poznanski, 2010). As shown in Section 2.1, given $(L_{\rm bol}, z, b, \Delta t, \epsilon_{\rm bk})$ we can simulate a GRB event. The distribution functions of these parameters have been determined. In this Section the form and parameters of these functions will be described. The data set used for comparison in this section is taken from Butler et al. (2007); Butler, Bloom & Poznanski (2010). For all cases a criterion of signal-to-noise ratio of $S/N > 10$ is applied. In cases where redshift information is needed (e.g. Luminosity function, redshift distribution), the redshift data are further selected using the criteria suggested by Jakobsson et al. (2006). These criteria select only redshifts measured under favorable conditions such that the distance is reliably measured. These criteria include the public availability of X-ray positioning within 12 hours; low Galactic foreground, i.e. $A_V < 0.5$; the burst took place no less than 55° from the Sun; no nearby bright star; and the burst should not be located at a polar declination, i.e. $|\delta| < 70^\circ$.

A catalog of GRBs[1] passing these redshift measurement criteria is then used to select *Swift* measurements. At the end of this selection procedure, 89 GRBs with high-quality measurements and redshift information is obtained.

[1] Available at http://www.raunvis.hi.is/~pja/GRBsample.html.

5.1.1 GRB luminosity function

The GRB luminosity function $\phi(\log L)$ is traditionally defined as the probability to find a GRB in a luminosity interval between $\log L$ and $\log L + d\log L$. This function is usually assumed to be of the form of a smoothly broken power law:

$$\phi(\log L) = \frac{dN}{d\log L} = \begin{cases} \left(\frac{L}{L_{\rm pk}}\right)^{-a_L} & \text{for } L \leq L_{\rm pk}, \\ \left(\frac{L}{L_{\rm pk}}\right)^{-b_L} & \text{for } L > L_{\rm pk}. \end{cases} \tag{5.1}$$

This function is normalized to the interval from zero to infinity. Recent results from *Swift* indicates that the bolometric luminosity function is well-described by the indices $(a_L, b_L) = (0.27, 3.46)$ and the peak luminosity $\log L_{\rm pk} = 52.95$ (Butler, Bloom & Poznanski, 2010). Figure 5.1 shows the luminosity function compared to a histogram of 89 *Swift* GRBs with measured redshift (Butler et al., 2007; Butler, Bloom & Poznanski, 2010). The bolometric luminosity $L_{\rm bol}$ is calculated using Equation 9 in Butler, Bloom & Poznanski (2010).

5.1.2 The distribution of burst duration T_{90}

The commonly used definition for the burst duration is T_{90}, defined as the time interval in which the background-substracted integrated counts from the GRB increase from 5% to 95% of the total counts (Kouveliotou et al., 1993, 1996). Based on this parameter, Kouveliotou et al. (1993) found a bimodality in the distribution of $\log T_{90}$ and thus introduced two distinct groups of GRBs: The short and the long duration GRBs, with T_{90} shorter or longer than 2 seconds.

Further analysis using the BATSE 3B catalog (Meegan et al., 1996), however, exhibit a possibility that the distribution of $\log T_{90}$ can also be well-fitted using a trimodal Gaussian thus indicating the existence of a third, intermediate, class of GRB (Horváth,

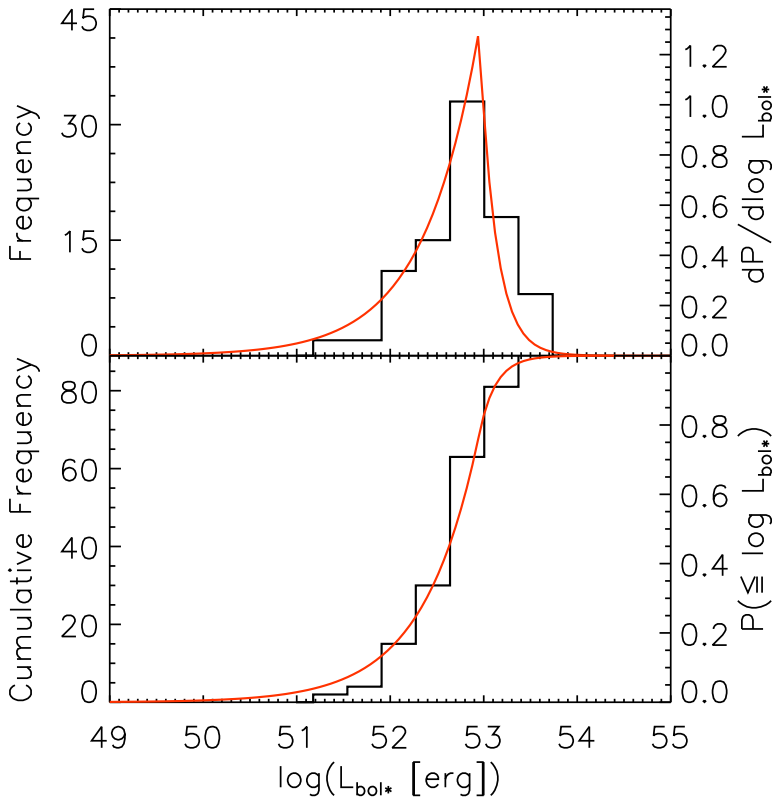

Figure 5.1: The top graph shows the luminosity probability density function while the bottom graph is the cumulative probability function. Red curves represent the best-fit GRB world model for the luminosity function (Butler, Bloom & Poznanski, 2010), compared to 89 selected *Swift* data with measured redshift (Butler et al., 2007; Butler, Bloom & Poznanski, 2010) and passing the redshift measurement criteria suggested by Jakobsson et al. (2006). The left side of the vertical axis is the actual number of data in each bin while the right side is the value of the probability function.

1998). Various statistical methods applied to different data sets from different satellites (e.g. BATSE (Horváth et al., 2006), BeppoSAX (Horváth, 2009), *Swift* (Horváth et al., 2008)) seem to indicate that this third class is real and not an artifact or bias from one particular satellite. While the short and long GRB can be explained as two distinct physical phenomena, the third class is still lacking any physical interpretation.

A trimodal Gaussion function is used to model the distribution function of $\log T_{90}$:

$$\frac{dN}{d\log T_{90}} = \sum_{k=s,l,i} \frac{w_k}{\sigma_k\sqrt{2\pi}} \exp\left[-\frac{\log^2(T_{90}/\log\mu_{T_{90},k})}{2\sigma_k^2}\right], \qquad (5.2)$$

in which (s, l, i) is the notation for respectively the short, long, and

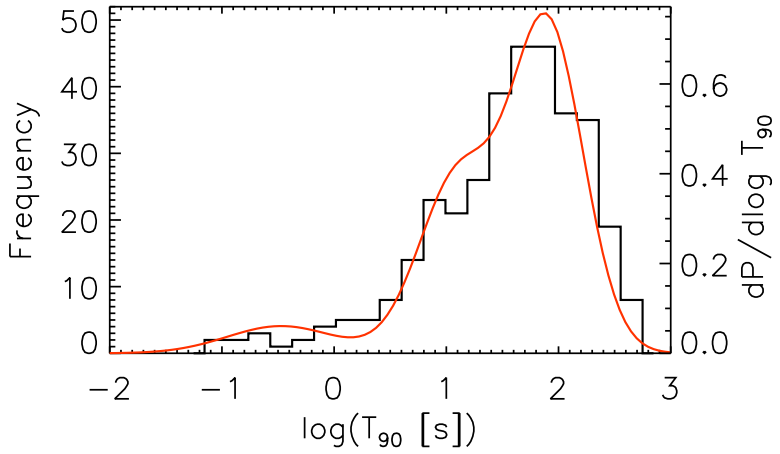

Figure 5.2: The red curve is the T_{90} distribution function from Horváth et al. (2008) compared to 345 T_{90} measurement by *Swift* (Butler et al., 2007; Butler, Bloom & Poznanski, 2010) with signal-to-noise ratio larger than 10. The parameters for the distribution function is shown in Table 5.1.

Terms	k subscript	$\mu_{T_{90},k}$	σ_k	w_k
short	s	-0.473	0.48	0.073
long	l	1.903	0.32	0.582
intermediate	i	1.107	0.35	0.345

Table 5.1: The parameters for the trimodal Gaussian distribution function of $\log T_{90}$ (Horváth et al., 2008).

intermediate duration GRB, w_k is the weight of the Gaussian function where $w_s + w_i + w_l = 1$ applies, $\mu_{T_{90},k}$ is the mean in $\log T_{90}$ and σ_k is the standard deviation. We use the parameters calculated by Horváth et al. (2008) for the *Swift* data, shown in Table 5.1. In Figure 5.2 the distribution function is shown alongside the T_{90} data measured by *Swift*. There are 345 *Swift* GRB measurement with signal-to-noise ratio $S/N > 10$. The lack of a physical interpretation for the intermediate class should not be a concern because the aim of this study is to accurately simulate the observational features and not to deduce any physical interpretation of these features.

5.1.3 *The instrinsic peak energy $\epsilon_{\mathrm{pk}*}$ distribution*

The intrinsic peak energy $\epsilon_{\mathrm{pk}*}$ is the energy in which the νf_ν spectrum peaks. It is calculated by performing a spectral fit to the measured energy spectrum of a GRB. What one obtains from this procedure is the observed peak energy ϵ_{pk}. For the Band spectrum

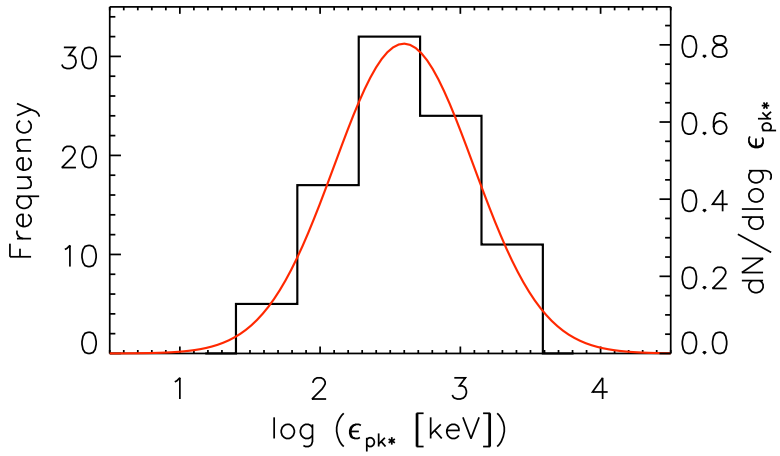

Figure 5.3: The logarithm of intrinsic peak energy ϵ_{pk*} histogram of 89 *Swift* GRB with measured redshift (Butler et al., 2007; Butler, Bloom & Poznanski, 2010). The histogram is compared to a best-fit Gaussian function in $\log \epsilon_{pk*}$.

(Equation 2.52), the peak energy is related to the break energy ϵ_{bk} through

$$\epsilon_{bk} = \frac{b-a}{1-a}\epsilon_{pk}. \tag{5.3}$$

The distribution function of ϵ_{pk*} can be modelled reasonably well by the normal distribution in $\log \epsilon_{pk*}$:

$$\frac{dN}{d\log \epsilon_{pk*}} = \frac{1}{\sqrt{2\pi\sigma^2_{\epsilon_{pk*}}}} \exp\left[-\frac{\log^2(\epsilon_{pk*}/\epsilon_{pk*,0})}{2\sigma^2_{\epsilon_{pk*}}}\right]. \tag{5.4}$$

The mean and variance of the distribution is found to be $(\log \epsilon_{pk*,0}, \sigma_{\epsilon_{pk*}}) = (2.58 \pm 0.05, 0.50 \pm 0.03)$. The corresponding function is shown as the red curve in Figure 5.3.

5.1.4 *The redshift distribution of GRBs in the universe*

The redshift distribution function is calculated using the physical model formulated by Le & Dermer (2007), which includes the effects of beaming by incorporating a distribution function for the jet opening angle. This model sets out by assuming a GRB energy

spectrum $\nu F_\nu = \epsilon^2 N(\epsilon)$ in the form of a broken power law, i.e.

$$\nu F_\nu \equiv f_{\epsilon_{\rm pk}} \left[H(\epsilon_{\rm pk} - \epsilon) \left(\frac{\epsilon}{\epsilon_{\rm pk}} \right)^{\alpha} + H(\epsilon - \epsilon_{\rm pk}) \left(\frac{\epsilon}{\epsilon_{\rm pk}} \right)^{\beta} \right], \quad (5.5)$$

where $\alpha(> 0)$ and $\beta(< 0)$ are the spectral indices of the energy spectrum, $\epsilon_{\rm pk}$ is the peak energy, and $H(x)$ is the Heaviside function. Using this energy spectrum, just as in Equation 2.54, we can calculate the bolometric fluence of the GRB:

$$F = \int_0^{\Delta t} dt \int_0^{\infty} d\epsilon \frac{\nu F_\nu}{\epsilon} = \lambda_{\rm bol} f_{\epsilon_{\rm pk}} \Delta t, \quad (5.6)$$

where the bolometric correction $\lambda_{\rm bol}$ in this is case is simply $\lambda_{\rm bol} = (\alpha^{-1} - \beta^{-1})$. Following Le & Dermer (2007), here the bolometric correction is always taken to be $\lambda_{\rm bol} = 5$ to simplify the situation.

Taking into account beaming effects, which means that the burst is collimated to a bipolar jet with opening angle θ_j, the beaming-corrected energy release $L_{\gamma *}$ is given by

$$L_{\gamma *} = 4\pi r_L^2 (1 - \cos\theta_j) \frac{F}{1+z}, \quad (5.7)$$

where r_L is the luminosity distance, related to the comoving distance as $r_L = (1+z) r_c$. Inserting Equation 5.6 into Equation 5.7, the peak flux is then given by

$$f_{\epsilon_{\rm pk}} = \frac{L_{\gamma *}}{4\pi r_L^2(z)(1 - \cos\theta_j)\Delta t_* \lambda_{\rm bol}}. \quad (5.8)$$

The number of GRB events per unit redshift per unit solid angle with spectral flux greater than $f_{\epsilon_{\rm pk}}$ can then be calculated using the formula

$$\frac{dN(> f_{\epsilon_{\rm pk}})}{d\Omega dz} = \frac{c}{H_0} \Theta(z) \frac{n_c(z) r_L^2(z)}{(1+z)^3 \sqrt{\Omega_\Lambda + \Omega_m (1+z)^3}}, \quad (5.9)$$

where $\Theta(z)$ is the jet opening angle distribution integrated over all possible opening angle:

$$\Theta(z) = \int_{\cos\theta_{j,\rm max}}^{\cos\theta_{j,\rm min}} d\cos\theta_j \; g(\cos\theta_j)(1 - \cos\theta_j). \quad (5.10)$$

The form for the jet opening angle distribution $g(\cos\theta_j)$ is unknown, but Le & Dermer (2007) consider the form

$$g(\cos\theta_j) = g_0(1-\cos\theta_j)^s H(\cos\theta_j;\cos\theta_{j,\max},\cos\theta_{j,\min}), \quad (5.11)$$

where s is the power-law index of $g(\cos\theta_j)$ and $H(x;a,b)$ is the Heaviside function such that it is $H(x;a,b)=1$ when $a \leq x \leq b$ and zero elsewhere. This distribution is normalized to unity, thus

$$g_0 = \frac{1+s}{(1-\cos\theta_{j,\max})^{1+s} - (1-\cos\theta_{j,\min})^{1+s}}. \quad (5.12)$$

The final form of the GRB rate per unit redshift per spatial opening angle is then (Le & Dermer, 2007)

$$\frac{dN(>f_{\epsilon_{\rm pk}})}{d\Omega dz} = \frac{cg_0}{H_0(2+s)} \frac{n_c(z) r_L^2(z)}{(1+z)^3\sqrt{\Omega_\Lambda + \Omega_m(1+z)^3}} \times \left\{ \left[1-\max(\hat{\mu}_j,\mu_{j,\min})\right]^{2+s} - (1-\mu_{j,\max})^{2+s} \right\}, \quad (5.13)$$

here $\mu_j = \cos\theta_j$ and

$$\hat{\mu}_j \equiv 1 - \frac{L_{\gamma *}}{4\pi r_L^2(z)\Delta t_* \hat{f}_{\bar{\epsilon}} \lambda_{\rm bol}}, \quad (5.14)$$

where $\hat{f}_{\bar{\epsilon}}$ is the νF_ν flux threshold sensitivity of *Swift*, taken to be $\hat{f}_{\bar{\epsilon}} = 10^{-8}$ erg cm^{-2} s^{-1}.

The function $n_c(z)$ is the comoving star formation rate from Hopkins & Beacom (2006) which is in the form of

$$n_c(z) = \frac{1+(a_2 z/a_1)}{1+(z/a_3)^{a_4}}, \quad (5.15)$$

where $a_1 = 0.015$, $a_2 = 0.10$, $a_3 = 3.4$, and $a_4 = 5.5$ are the best-fit parameters (Le & Dermer, 2007).

The unknown parameters in Equation 5.13 can be calculated by performing a fit of the function to the observed GRB redshift distribution. Le & Dermer (2007) obtained a best-fit values of $L_{\gamma *} = 4\times 10^{51}$ ergs, $\theta_{j,\min} = 0.05$ rad, $\theta_{j,\max} = 0.7$ rad, and $s = 1.25$. The form of the function with the best-fit values is shown

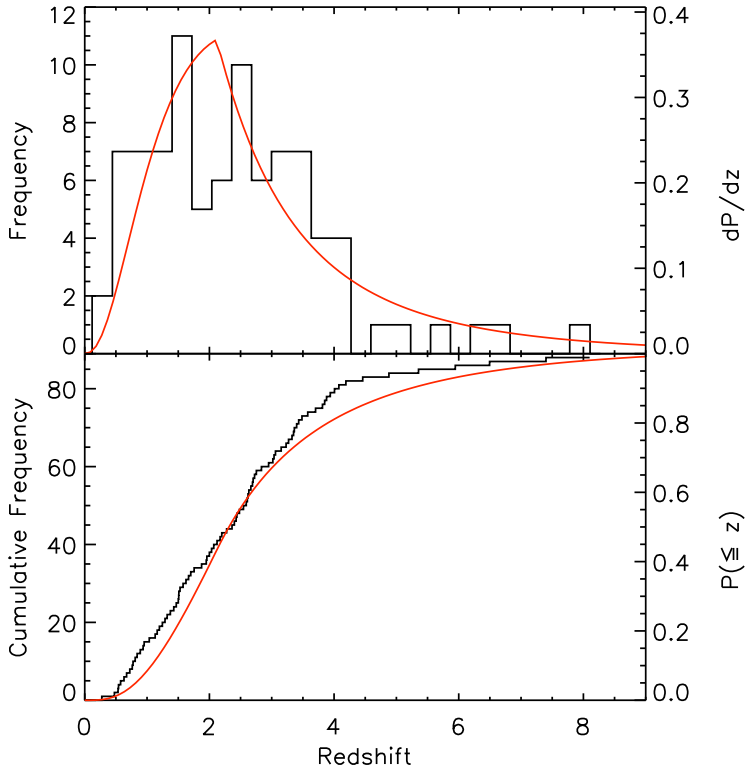

Figure 5.4: The GRB redshift distribution compared to the distribution function of Le & Dermer (2007). The best-fit values of $L_{\gamma*} = 4 \times 10^{51}$ ergs, $\theta_{j,\min} = 0.05$ rad, $\theta_{j,\max} = 0.7$ rad, and $s = 1.25$ are used.

in Figure 5.4, as compared to the observed redshift distribution.

With this distribution function, we can estimate the probability to observe a GRB of redshift $z \lesssim 0.1$. Figure 5.5 shows a more detailed view of Figure 5.4 in low-redshift area. Le & Dermer (2007) estimated that the probability to observe a GRB of redshift $z \lesssim 0.1$ is $P(z \leq 0.1) \sim 7 \times 10^{-5}$, and that $P(z \leq 0.2) \sim 6.5 \times 10^{-4}$. Assuming that 1 GRB is detected per day by any satellites, from these number we can expect to observe 1 GRB with $z \leq 0.1$ every $\sim$40 years and 1 GRB every $\sim$4.2 years to have a redshift of $z \leq 0.2$. The second number is still within the expected operation time of neutrino telescopes, which is approximately 5–10 years.

Despite these discouragingly low numbers predicted by theo-

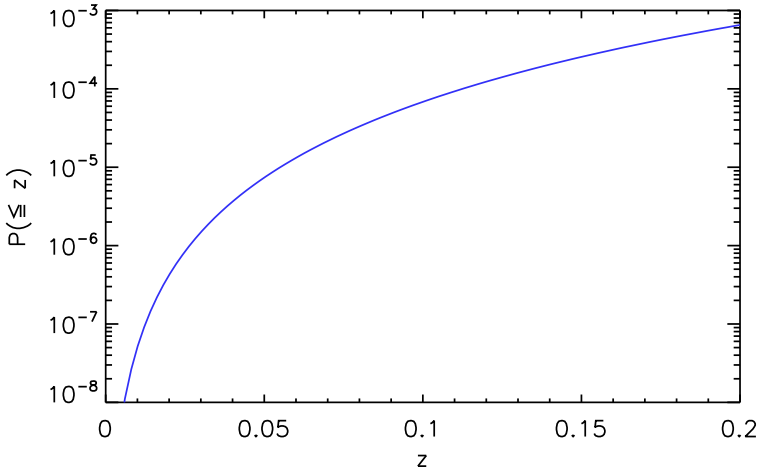

Figure 5.5: A more detailed view of the GRB redshift distribution function of Le & Dermer (2007) for low-redshift area.

retical calculations, in the last 14 years we have observed at least 6 GRBs with $z \leq 0.1$ and 12 GRBs with $z \leq 0.2$ within the same time period[2]. These facts alone show us the still-uncertain nature of the GRB redshift distribution and that this venture is still worth-pursuing.

[2] From the GRB index of GRBox, http://lyra.berkeley.edu/grbox, retrieved on August 30 2012.

5.2 *GRB event generation and muon flux calculations*

Generations of GRB events are performed for several data taking period (in years) $n_{\mathrm{yr}} = \{1, 2, 3, 5, 10\}$ yr. It assumed that 1 GRB is detected per day, thus making the number of GRBs generated to be $n_{\mathrm{GRB}} = 365 \times n_{\mathrm{yr}}$. For each data taking period, each GRB is generated by randomly generating the six parameters using the inverse-transform method (Nakamura & Particle Data Group, 2010). The zenith distance $\cos\theta$ of each GRB is randomly generated assuming an isotropic spatial distribution in the sky. The azimuth angle is not generated as it does not have any effect on the resulting muon spectrum.

Only GRBs above the horizon are then selected for further calculations. the six parameters $(L_{\mathrm{bol}}, z, b, \Delta t, \epsilon_{\mathrm{bk}}, \theta)$ is then used to calculate the muon spectrum at detector depth $d = 2475$ km, following the prescriptions described in Chapters 2–3.

The on-period of each GRB observation is defined to be equal to T_{90} and the off-period is taken to be 1 hour before the GRB took place, at the same zenith distance as the observed GRB. The number of expected event at detector depth could then be calculated, and the number of expected background during the off-period.

The total number of events from GRBs above the horizon during the observation period are then summed, thus stacking all observed sources as if they are a single observation. The significance S of the observation during the data-taking period is then calculated using the Li & Ma (1983) significance formula written in Equation 4.2.

Due to the stochastic nature of GRB events, this simulation is repeated 10^6 times in order to analyze the distribution of the significance and to estimate the discovery potential.

5.3 *Result and conclusions*

THE RESULT of the simulation is shown in Figure 5.6. Each panel in the Figure describes the probability do make a detection with significance greater than any given S, for 4 different detector size (i.e. $A_\mu^{\text{eff}} = \{10^{-3}, 10^{-2}, 0.1, 1\}$ km^2) and for 5 different data-taking period.

The result in Figure 5.6 indicates that an ANTARES-sized detector of $A_\mu^{\text{eff}} = 10^{-2}$ km^2 is still too small make a discovery. Even a sub-km^3 detector with $A_\mu^{\text{eff}} = 0.1$ km^2 still has very little chance to make a discovery with at 3σ significance, as it has only 5% probability of making a 3σ discovery or better (for a data-taking period of 5 years).

A km-sized detector can have a better chance of making a 3σ detection. After an operation of 5 years, it has $\sim$50% probability to detect TeV photon signals with 3σ significance or better, and $\sim$25% probability for a 5σ detection or better.

From these results it can be safely concluded that a neutrino telescope that can be taken seriously must have an instrumented volume of at least 1 km^3, which enables it not only to detect astrophysical high-energy neutrinos but also plays its secondary role as a VHE γ-ray observatory.

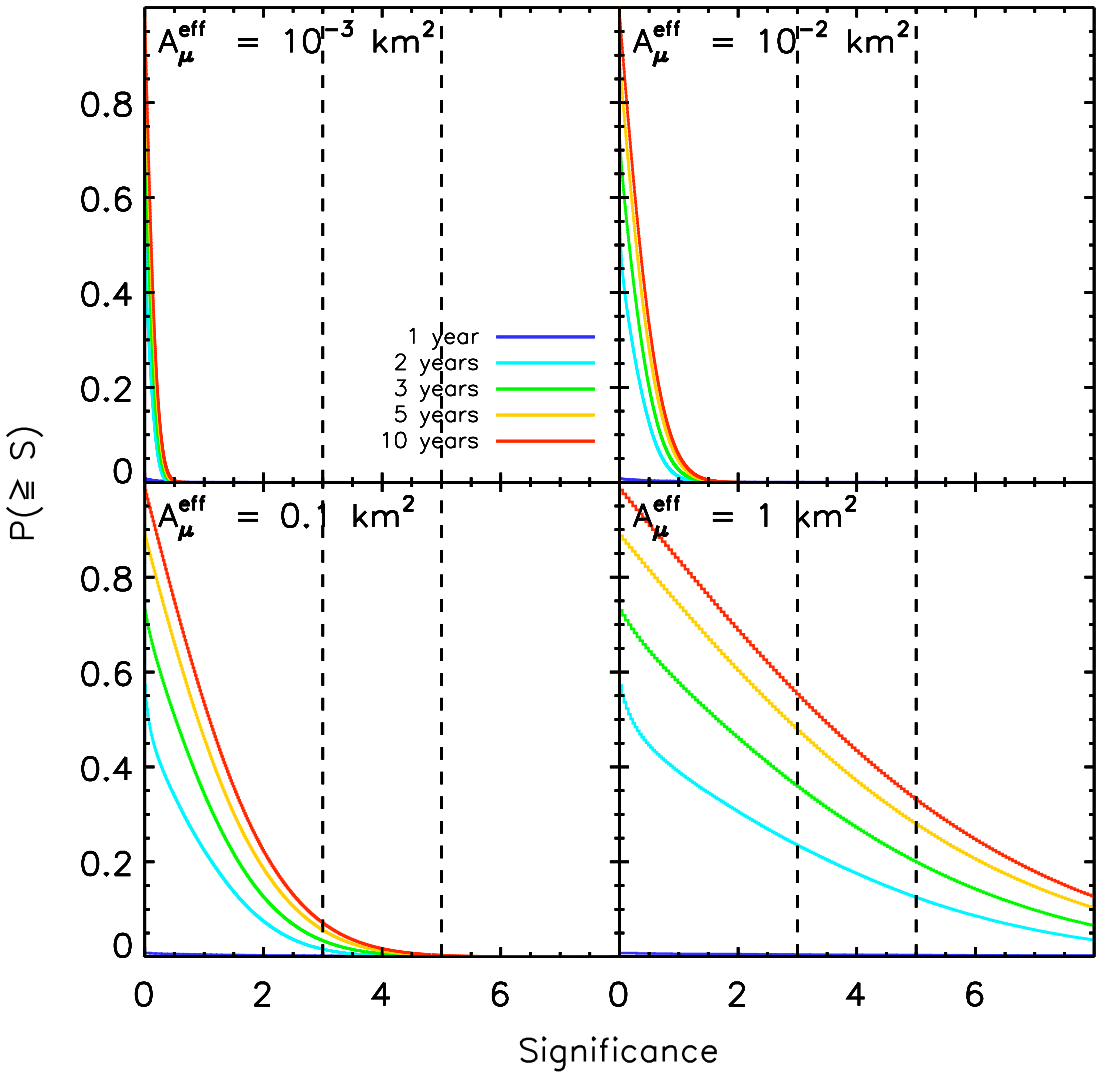

Figure 5.6: The distribution of the detection significance S of stacked GRB observations, here plotted for four different detector size and 5 different data-taking period. The larger the detector size, the better the chance to detect events with 3σ and 5σ significance or better, as indicated by the dashed vertical lines.